This paper appears in Journal of Medical Robotics Research, 2018
DOI: 10.1142/S2424905X18410040

Model Averaging and Input Transformation for 3D Needle Steering*

Bita Fallahi[a,†], Ron Sloboda[b,‡], Nawaid Usmani[b,‡], Mahdi Tavakoli[a,†]

[a] *Department of Electrical and Computer Engineering, University of Alberta, Edmonton, Canada T6G 1H9*
E-mail: fallahi@ualberta.ca

[b] *Cross Cancer Institute and the Department of Oncology, University of Alberta, Edmonton, Canada T6G 1Z2*

In this paper, a duty-cycle based method is proposed for needle steering in 3D. The paper models the continuous 3D needle steering problem as a four-mode switching system and provides a new average-based formulation to transform the continuous input into a switching sequence. In this structure, the needle tip deflection control system is decomposed to two different 2D subsystems. Each subsystem has its own input, for which a controller can be designed to adjust a switching duty cycle. The duty cycles from the two subsystems are then combined to provide an axial needle rotation command to control the needle deflection in 3D. In order to show the application of the proposed formulation, robust sliding mode technique is employed to design controllers for each subsystem and, thus for the total system in 3D. The controllers are designed to be robust with respect to uncertainties in the value of the needle path curvature and to deal with measurement limitations. The performance of the proposed framework is shown by performing experiments in different scenarios.

Keywords: Needle steering; switching; sliding mode

1. Introduction

Needle steering involves the insertion of long flexible needles into the human body for diagnosis, therapeutics delivery or sample removal. In some procedures such as biopsy, the goal is to steer the needle to a target point, regardless of the path travelled by the needle. In some other applications, such as brachytherapy, and in presence of the obstacles, the goal is to steer the needle to follow a pre-planned path. In all of these procedures, the efficiency of the procedure depends on the needle tip positioning accuracy. The efficiency of these methods can be improved by employing intelligent assistant robots to compensate for needle tip positioning errors and improve performance [1].

As a beveled-tip needle is inserted into the tissue, due to the asymmetric forces at the needle tip [2], the needle bends. The path travelled by the needle depends on the orientation of the bevel, which changes by needle axial rotations and provides a way for steering the needle on different paths. The desired path, however, depends on the application. In biopsy it is desired to reach a constant final deflection whereas in brachytherapy the needle should follow a straight path. In case of having obstacles on the needle path (such as bones or nerves) the needle should follow a pre-planned curved path. In this paper the main focus is on needle steering for brachytherapy and obstacle avoidance.

Needle deflection at each depth of insertion can be projected on two planes, representing in-plane and out-of-plane motion. From this point of view, the needle represents an under-actuated system as there are two objectives; controlling the in-plane and out-of-plane deflections while there is only one control input, the needle axial rotations. This along with some non-holonomic constraints imposed on the needle kinematics turns the needle steering procedure into a challenging control problem, for which many different plan-

*This work was supported by the Natural Sciences and Engineering Research Council (NSERC) of Canada under grant CHRP 446520, the Canadian Institutes of Health Research (CIHR) under grant CPG 127768, and by the Alberta Innovates - Health Solutions (AIHS) under grant CRIO 201201232.

†E-mail: {fallahi, mahdi.tavakoli}@ualberta.ca

‡E-mail: {ron.sloboda, nawaid.usmani}@albertahealthservices.ca.

ning and control strategies have been proposed in the literature.

Beveled-tip needles can be steered on different paths using needle axial rotations.As shown in Fig. 1, rotating the needle at some depth, changes the bevel orientation and consequently the path the needle moves on. In [3], duty-cycle-based spinning is proposed to achieve paths with different curvatures. In this method, which is based on simultaneous insertion and rotation of the needle, the duty cycle, which determines the time intervals of pure insertion and simultaneous insertion and rotation, is found as a function of the desired path curvature. There are different needle steering methods based on the duty-cycle-based spinning of the needle. Authors in [4] have proposed solutions to overcome hardware limitations in the duty-cycling method. Authors in [5] have used a rapid re-planning strategy to plan and control needle movement toward a desired location while avoiding obstacles. In this method, the needle is steered using duty-cycle spinning where the empirical relation between the needle's path curvature and the duty cycle is found by fitting polynomials to experimental data. The work done in [6] is also based on the rapidly exploring random tree algorithm, which allows the planned trajectories to be composed of circular arcs of bounded curvature. The desired path is then followed using duty cycle spinning. In [7], an adaptive steering method is proposed in which the needle's path curvature estimation and the duty cycle spinning are integrated to steer the needle to the desired location. In [8], needle entry point planner is proposed and is combined with an intraoperative robust planning method to compensate for parameter uncertainties and disturbances. Using the affine relationship between the needle path curvature and duty cycle, the needle is steered through the desired path. In [9] a mechanics based model and a controller are proposed for controlling the needle tip position. The controller is combined with duty cycle spinning to reduce the needle curvature whenever needed. In [10], a new duty cycle spinning method is proposed, which moves the needle on 3D non-planar trajectories using visual servoing. This method is also used in [11], in which a new needle tracking algorithm is proposed.

This paper provides a new formulation for modelling the 3D needle steering problem as a four-mode switching system which can be implemented in a PWM framework. Using a PWM framework, the average of the switched system represents the behaviour of the real system in which the duty cycle is considered as the continuous input to the system [12]. However, the approach for finding the duty cycle is different from methods proposed in the literature. This work is a 3D extension of the method proposed in [13], in which the system is considered as a two-mode switching system for a 2D steering problem, i.e., inserting the needle and control the deflection in one plane. Here, the same idea is employed and the system is considered as a four-mode switching system for steering the needle in a 3D environment to control the in-plane and out-of-plane deflection. This new formulation provides a way to utilize different control strategies proposed in the literature and to implement those strategies through a PWM framework.

1.1. *Contributions*

In order to use the idea of switching proposed in [13] in a 3D environment, the continuous 3D system is mapped as two, 2-mode switching subsystems with virtual inputs for in-plane and out-of-plane motions. If each discrete subsystem represents the system in a defined interval in a PWM period, time-averaging all subsystems across the PWM period can be representative of the original subsystem. This formulation provides a map between the binary-input subsystems and their duty cycle. The duty cycles of both subsystems are then combined to form a multi-mode PWM structure. Viewing the duty cycle as a virtual continuous input provides a means for using different control strategies proposed in the literature for controlling a needle in 3D. Any controllers designed for the continuous-input time-averaged systems that satisfy the system constraints and provide a good performance can be used in this framework. In this PWM framework different discrete modes are considered for the system. Switching between these modes does not require accurate measurement of the needle tip orientation, which itself is a challenging problem. Methods in the literature, in which the needle tip orientation is used for finding the control action [14], require needle tip orientation sensors, however, using needle mounted sensors is not clinically feasible.

The PWM structure proposed in this paper is different from the duty-cycle based methods used in the literature. In the duty-cycle spinning [3] or flipping [4], the duty cycle period is adjusted to control the desired path curvature and the duty cycle determines the time intervals for pure insertion and simultaneous insertion and rotation. During the insertion in these methods, if errors occur due to tissue non-homogeneity or uncertainties, re-planning is required to find a new desired path to compensate for the errors. According to the new formulation in this paper, however, the duty cycle serves as a virtual continuous input for each subsystem, which does not require any empirical relations between the duty cycle and the needle path curvature. In this case, the duty cycle determines the time intervals for any of defined modes for the multi-mode system. Considering the duty cycle as the continuous input for each subsystem, closed-loop feedback control strategies can be used to compensate for the deflection errors.

In order to have a general comparison, it should be noted that from a feedback control perspective, the needle system suffers from under actuation as there is one control input; the needle axial rotation, and two control outputs; needle deflection in two directions or equivalently in- and out-of-plane motions. Using this formulation, the 4 mode switching method provides a way to control the in- and out-of-plane motions simultaneously. As stated above, the proposed method is different from duty cycling. Compared to the motion planning methods, in which the errors are compensated through re-panning, the proposed struc-

ture is computationally less expensive as the error is compensated by the controller in a feedback loop. Moreover, this method provides a framework to be used with different control strategies. Considering the constraints imposed by model averaging, controllers are to be designed for the averaged subsystems, which can be implemented using the switching framework.

In the second part of the paper, the proposed time-averaged formulation is used to design controllers for each subsystem. Due to limitations in measuring all system states (such as the needle tip orientation) using ultrasound images and the uncertain value of the needle path curvature, the averaged system is rewritten as a nominal system with bounded uncertainties. The controllers are designed based on sliding mode technique which provide a robust design in counteracting modelling and parametric uncertainties. Using a Lyapunov function candidate, the convergence of the proposed sliding mode controllers is demonstrated for the uncertain subsystems. The designed controllers provide an application of the averaged model while other controllers which can deal with the uncertainties and limitations of the system and provide a good performance for the averaged subsystems can also be used as the rotation pattern is independent of the controller. The main goal of this research is to study the feasibility of the proposed method for steering the needle on a straight path with the application in brachytherapy, however, it is shown that the proposed structure is not limited to this special case and can be also used for obstacle avoidance needle steering.

The paper is organized as follows: In section 2, the subsystems and the four-mode switched system are introduced. In section 3, the sliding mode controllers are presented, and section 4 presents the experimental results.

2. Switched System

2.1. *Needle kinematics*

The coordinate free kinematics of a beveled-tip needle is proposed in [15], in which the motion of the needle tip in soft tissue is assumed to be the same as the motion of a bicycle with fixed front wheel angel. Using the vector $\mathbf{q} = [x,\, y,\, z,\, \alpha,\, \beta,\, \gamma]^T$ as the generalized coordinates which is well defined on $\mathcal{U} = \{\mathbf{q} \in \mathbb{R}^6 : \alpha, \gamma \in \mathbb{R}, \beta \in [-\pi/2, \pi/2]\}$, the needle kinematics can be presented as: [16]

$$\dot{x} = v \sin\beta \tag{1a}$$
$$\dot{y} = -v \cos\beta \sin\alpha \tag{1b}$$
$$\dot{z} = v \cos\alpha \cos\beta \tag{1c}$$
$$\dot{\alpha} = kv \cos\gamma \sec\beta \tag{1d}$$
$$\dot{\beta} = kv \sin\gamma \tag{1e}$$
$$\dot{\gamma} = -kv \cos\gamma \tan\beta + u \tag{1f}$$

Here, $\dot{()}$ denotes the time derivative and $[x \;\; y \;\; z]^T$ represents the position of the origin of the moving frame $\{B\}$ attached to the needle tip with respect to the fixed frame $\{A\}$ as shown in Fig. 1. The angels α, β and γ are the yaw, pitch, roll angles, representing the orientation of the frame $\{B\}$ with respect to frame $\{A\}$. Using these three angels, the orientation of the moving frame can be obtained by three successive rotations about the axes of the fixed frame. Since the rotations are performed about the fixed axes, the corresponding rotation matrix can be found by pre-multiplying of the three basic rotation matrices [17]. In these equations, k is the needle path curvature and v and u are the needle insertion velocity and needle axial rotational velocity, respectively.

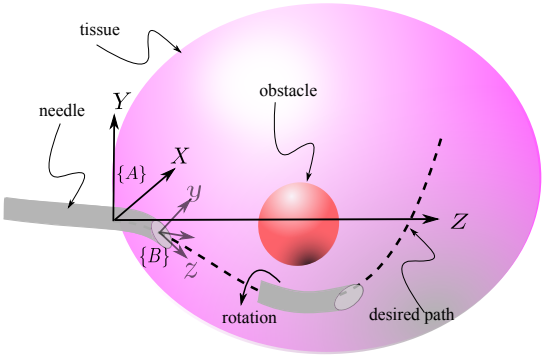

Figure 1. The 3D motion of needle, desired path and obstacle. Frames $\{A\}$ and $\{B\}$ are the fixed and the tip-attached moving frames, respectively. The rotation changes the bevel orientation to steer the needle on the desired path.

In our past work proposed in [13], it is assumed that the needle shaft remains in the $Y - Z$ plane, so there is no need for out-of-plane control. The desired position is then considered as a desired deflection in the y direction at a desired depth. In this case, the only two possibilities for the bevel orientation is the bevel pointing up or down, which defines the two-mode switching system.

The problem of needle tip positioning in the 3D space can be considered as having a desired deflection at a desired depth. The needle depth and deflection can be controlled using the insertion velocity v and the rotational velocity u. Here, the focus is on automatic control of the needle tip deflection using axial rotations as according to (1), the needle tip orientation is the key factor in determining the path travelled by the needle. In this approach, the needle insertion is considered as an independent manually-controlled degree of freedom, which provides the possibility of keeping the surgeon in the loop to increase the safety of the procedure. In this section, the needle kinematics are divided into two subsystems, projecting the needle tip deflection into two directions x and y. In (1), the rotational velocity u directly affects the roll angle γ, which itself indirectly influences the needle tip deflection in both directions. Assuming we have full control over γ through the input u and assuming the rotations are fast with respect to the insertion, the angle γ can be considered as the control input for the two 2D subsystems. The subsystems are defined independently with their own virtual inputs. Here, it is assumed the virtual inputs are completely independent, which is not

true as they both depend on the angle γ. This overlap is discussed and resolved later.

2.2. *Switched four-mode system*

For the 2D planar case, there are two possibilities for the bevel, assuming that the needle flips instantly [13]. In the 3D case, assuming γ can only take two fixed values apart by 180° in two opposing quadrants, each subsystem is defined as a two-mode switching system. The needle deflection dynamics in x direction can be written as

$$\dot{x} = v \sin\beta \tag{2a}$$

$$\dot{\beta} = (kv)\bar{u}_x \tag{2b}$$

or equivalently based on (1)

$$\ddot{x} = b_x \bar{u}_x \tag{3}$$

where $b_x = kv^2 \cos\beta$ and $\bar{u}_x = \sin\gamma^*$ with $|\sin\gamma^*|$ being constant and $\gamma^* \in [0, \pi]$ to have $\bar{u}_x > 0$, or $\gamma^* \in [\pi, 2\pi]$ to have $\bar{u}_x < 0$, representing the two switching modes. Assuming the switching happens according to the normalized PWM period $D_x = [d_x \;\; 1 - d_x]^T$ with $\|D_x\|_1 = 1$, the averaged system is obtained as

$$\ddot{x}_a = d_x b_x |\bar{u}_x| - (1 - d_x) b_x |\bar{u}_x| = b_x u_x \tag{4}$$

with

$$u_x = (2d_x - 1)|\bar{u}_x| \tag{5}$$

Similarly, for the y direction the subsystem equations can be written as

$$\dot{y} = -v \cos\beta \sin\alpha \tag{6a}$$

$$\dot{\alpha} = (kv) \sec\beta \bar{u}_y \tag{6b}$$

where $\bar{u}_y = \cos\gamma^*$ with $|\cos\gamma^*|$ being constant. γ^* can have only two values either in $[-\pi/2, \pi/2]$ to have $\bar{u}_y > 0$ or $[\pi/2, 3\pi/2]$ to have $\bar{u}_y < 0$. Using this, (6) can equivalently be written based on (1) as

$$\ddot{y} = f_y + b_y \bar{u}_y \tag{7}$$

with $f_y = kv^2 \sin\alpha \sin\beta \sin\gamma^*$ and $b_y = -kv^2 \cos\alpha$. Using the PWM period $D_y = [d_y \;\; 1 - d_y]^T$ with $\|D_y\|_1 = 1$, the time-averaged model of (7) can be written as

$$\ddot{y}_a = d_y(f_y + b_y|\bar{u}_y|) + (1 - d_y)(f_y - b_y|\bar{u}_y|) = f_y + b_y u_y \tag{8}$$

in which

$$u_y = (2d_y - 1)|\bar{u}_y| \tag{9}$$

In this format, u_x and u_y are continuous virtual inputs to be designed for the subsystems (4) and (8), respectively. Regardless of the control strategy used for calculating u_x and u_y, in order to use these signals in the switched control, these values should be converted to the duty cycles D_y and D_x using

$$d_i = \frac{(u_i/|\bar{u}_i| + 1)}{2} \qquad i = x, y \tag{10}$$

The values d_x and d_y determine the duty cycle for switching between the two modes in each subsystem. However, from (9) and (5), it is clear that u_y and u_x are not independent as they both depend on the value of γ^*. Since $\bar{u}_x$ and $\bar{u}_y$ depend on $\sin\gamma^*$ and $\cos\gamma^*$, respectively, it is possible to integrate the two 2-mode subsystems to build up a four-mode composite system. The four modes can be defined based on the fact that for each subsystem, γ^* is selected to be in a half-plane, i.e., up/down half plane for x direction and left/right half plane for y direction, as shown in Fig. 2. These four modes cover the four possibilities for $\sin\gamma^*$ and $\cos\gamma^*$ as each mode represents one quadrant in the plane. Through this selection, the magnitude γ^* can also be considered as a weighting parameter to change the magnitude of $\bar{u}_x$ and $\bar{u}_y$. If $|\tan\gamma| = 1$, the weights over x and y directions are equal; however, it is possible to emphasize on error in x and y directions by selecting $|\tan\gamma^*| > 1$ and $|\tan\gamma^*| < 1$, respectively. Since the duty cycles D_x and D_y determine the time required for the system to stay in each mode, in one cycle, the system uses a maximum number of three of the four available modes. The switching sequence can be performed according to the time required for each direction as shown in Table 1.

Table 1. The four-mode switching pattern based on the duty cycle

	$d_x > d_y$			$d_y > d_x$		
time	d_y	$d_x - d_y$	$1 - d_x$	d_x	$d_y - d_x$	$1 - d_y$
mode	**1**	**2**	**3**	**1**	**4**	**3**

Using this formulation, any continuous control law u_y and u_x which provide the desired performance for the averaged subsystems can be transformed into duty cycles D_y and D_x using (9) and (5). This provides the possibility of using different control strategies and translating them into a switching framework for steering the needle to the desired position. In the next section, the sliding mode technique is employed for controlling the two subsystems. Due to the uncertainties in the system parameters and the presence of non-measurable states, sliding mode control provides a robust approach for overcoming the uncertainties and disturbances while reaching the desired performance.

This formulation is based on the assumption that the angle γ can accurately be controlled to the desired value γ^*. However, since the orientation of the needle cannot be measured using ultrasound images, accurate measurement of this angle is not possible. However, since clinically used needles (also used in this paper) are torsionally highly stiff and also the curvature for these needles is very small, considering some bounds on the orientation angels, we have assumed that angle γ is equal to the needle base angel.

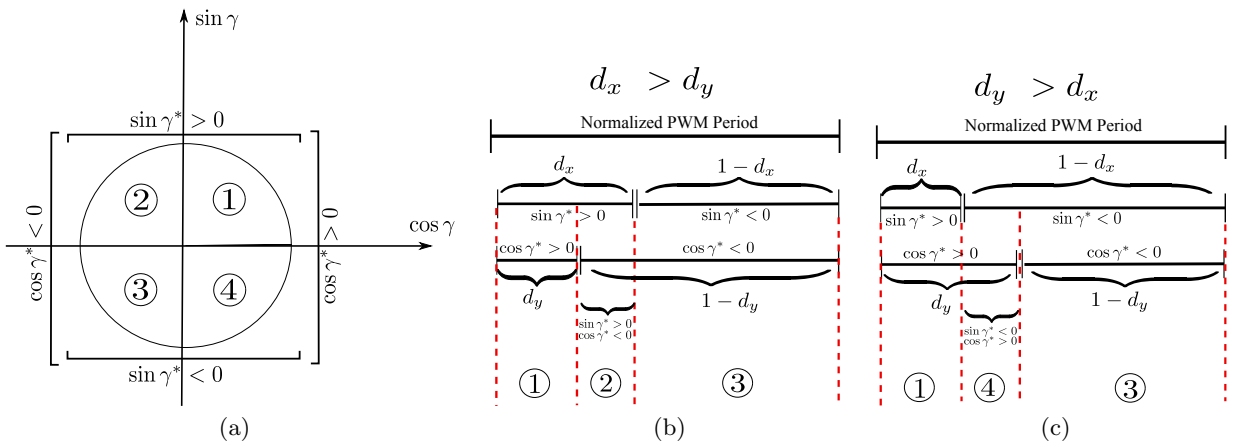

Figure 2. The switching pattern for the combined four-mode system. (a): Half planes representing two modes for each subsystem and the corresponding four modes: 1) $\sin\gamma^* > 0, \cos\gamma^* > 0$, 2) $\sin\gamma^* > 0, \cos\gamma^* < 0$, 3) $\sin\gamma^* < 0, \cos\gamma^* < 0$, 4) $\sin\gamma^* < 0, \cos\gamma^* > 0$. (b): The switching pattern when $d_x > d_y$. (c): The switchin pattern when $d_y > d_x$

3. Controller

While the average transformed model can be used with more than one control method, we use sliding mode control to show the utility of the averaged model. From equations (8) and (4), the needle path curvature k enters in the subsystem equations. This parameter depends on needle and tissue properties, which due to tissue in-homogeneity, encounters uncertainties. However, this parameter can be considered as a bounded uncertain parameter, with bounds determined by pre-operative tests. Moreover, the angles α and β, representing the needle tip orientation, are also present in the system equations (1). Incorporating these angles in the control law requires good measurements or estimations of the needle tip orientation, which is not a trivial task and requires using orientation measurement sensors that are not compatible with clinical realities. Besides, the combination of a state observer with a feedback controller represents new challenges, which require additional analysis for ensuring the stability of the closed-loop system [18]. However, fortunately the orientation-dependent terms appear as bounded nonlinear functions, which can be considered as uncertainty around some nominal model.

Sliding mode control is a technique that provides high robustness with respect to the parametric uncertainties and other disturbances [19]. According to the uncertainties present in the system, i.e the uncertainty in the curvature and the effects of the bounded orientation terms, the sliding mode control technique seems to suit the requirement of the system. In this section, the nominal model and its associated uncertainties are presented for each subsystem and then a robust sliding mode controller is designed which guarantees the convergence of the uncertain equations.

3.1. *Uncertain model*

As stated before, the angles α and β are not measurable through ultrasound images. However, these values are considered to be bounded. In reality, due to the presence of the tissue and the limited curvature of the needles, α and β cannot go unbounded. In practice, larger values of these angles correspond to more needle bending, which depends on the desired path travelled by the needle, thus having a feasible desired trajectory for the needle also puts limits on α and β ranges. The limitation can be imposed in the path planing level. Therefore, it is assumed that $|\alpha| < \alpha^*$ and $|\beta| < \beta^*$, where $\alpha^*, \beta^* \in (0, \pi/2)$ which are determined according to the application in the path planning level. Besides, the value of the curvature k represents a bounded uncertain value as $\underline{k} < k < \bar{k}$. Using these bounds, b_y and b_x in (8) and (4) satisfy the following inequalities

$$\underline{k}v^2 \cos\beta^* \leq b_x \leq \bar{k}v^2 \tag{11a}$$

$$\underline{k}v^2 \cos\alpha^* \leq b_y \leq \bar{k}v^2 \tag{11b}$$

Defining $\hat{k}$, $\hat{b}_y$ and $\hat{b}_x$ as the geometric mean of the above bounds, i.e., $\hat{k} = \sqrt{\underline{k}\bar{k}}$, $\hat{b}_y = -\hat{k}v^2\sqrt{\cos\alpha^*}$ and $\hat{b}_x = \hat{k}v^2\sqrt{\cos\beta^*}$, and substituting in (4) and (8), the nominal subsystem in x direction can be expressed as

$$\hat{\dot{x}}_a = \hat{b}_x \hat{u}_x \tag{12}$$

with

$$\left(\frac{\underline{k}\cos\beta^*}{\bar{k}}\right)^{1/2} \leq \frac{\hat{b}_x}{b_x} \leq \left(\frac{\bar{k}\cos\beta^*}{\underline{k}}\right)^{1/2} \tag{13}$$

Similarly, the nominal subsystem in y direction can be written as

$$\hat{\dot{y}}_a = \hat{f}_y + \hat{b}_y \hat{u}_y \tag{14}$$

with

$$|\hat{f}_y - f_y| \leq 2\bar{k}v^2 \tag{15a}$$

$$\left(\frac{\underline{k}\cos\alpha^*}{\bar{k}}\right)^{1/2} \leq \frac{\hat{b}_y}{b_y} \leq \left(\frac{\bar{k}\cos\alpha^*}{\underline{k}}\right)^{1/2} \tag{15b}$$

3.2. *Sliding mode controller*

Considering the y direction, the sliding surface S_y is defined as

$$S_y = \dot{e_y} + \omega e_y \tag{16}$$

with ω being a positive constant and $e_y = y - y_d$, where y_d is the desired deflection in y direction to be followed. Taking the time derivative of this sliding surface and substituting from (7) gives

$$\dot{S}_y = f_y + b_y u_y - \ddot{y}_d + \omega \dot{e}_y \tag{17}$$

This equation gives the equivalent control law for the averaged system, which makes the sliding surface to remain on zero.

Substituting (14) in (17) and solving $\dot{S}_y = 0$ for $\hat{u}_y$ gives

$$\hat{u}_y = \frac{1}{\hat{b}_y}\left(-\hat{f}_y + \ddot{y}_d - \omega\dot{e}_y\right) \tag{18}$$

However, this control law is only valid for the nominal system, which is different from the real system. This can be dealt with by changing the control signal in the following theorem:

Theorem 3.1. Consider system (8). Selecting $F_y = 2\bar{k}v^2$, $\lambda_y = \left(\frac{\bar{k}\cos\beta^*}{\underline{k}}\right)^{1/2}$ and $\eta > 0$, the control law

$$u_y = \hat{u}_y - \frac{1}{\hat{b}_y} K_y \text{sgn}(S_y) \tag{19}$$

with S_y defined in (16) and

$$K_y = \lambda_y(F_y + \eta) + (\lambda_y - 1)|\hat{b}_y\hat{u}_y| \tag{20}$$

ensure the convergence to the sliding surface $S_y = 0$.

Proof. Consider the Lyapunov candidate function

$$V_y = \frac{1}{2}S_y^2 > 0 \tag{21}$$

Taking time derivative of S_y and substituting from (8), (18) and (19) gives

$$\dot{S}_y = \left(f_y - \frac{b_y}{\hat{b}_y}\hat{f}_y - (1 - \frac{b_y}{\hat{b}_y})(\ddot{y}_d - \omega\dot{e}_y) - \frac{b_y}{\hat{b}_y}K\text{sgn}(S_y)\right) \tag{22}$$

Using (20), the above equation can be written as

$$\begin{aligned}\dot{S}_y = &-\text{sgn}(S_y)\left(-(f_y - \hat{f}_y)\text{sgn}(S_y) + \frac{b_y}{\hat{b}_y}\lambda_y F_y\right)\\ &- \text{sgn}(S_y)\left(|\hat{b}_y\hat{u}_y|(\lambda_y - 1 - (\frac{b_y}{\hat{b}_y} - 1)\text{sgn}(S_y)\text{sgn}(\hat{b}_y\hat{u}_y))\right)\\ &- \text{sgn}(S_y)\frac{b_y}{\hat{b}_y}\eta\end{aligned} \tag{23}$$

From (15), since $|f_y - \hat{f}_y| < F_y$ and $\lambda_y > \frac{b_y}{\hat{b}_y} > 1$, the above equations leads to

$$\dot{S}_y \leq -\eta\text{sgn}(S_y) \tag{24}$$

which by multiplying the sides of this inequality by S_y gives

$$S_y\dot{S}_y \leq -\eta|S_y| \tag{25}$$

which shows the finite time convergence of the sliding surface S_y. □

Similarly, for the x direction the sliding surface S_x is defined as

$$S_x = \dot{e}_x + \omega e_x \tag{26}$$

in which $e_x = x - x_d$ with x_d being the desired deflection in x direction and ω being a positive constant. The equivalent control law $\hat{u}_x$ is found as

$$\hat{u}_x = \frac{1}{\hat{b}_x}\left(\ddot{x}_d - \omega\dot{e}_x\right) \tag{27}$$

Theorem 3.2. Consider system (4). Selecting $\lambda_x = \left(\frac{\bar{k}\cos\beta^*}{\underline{k}}\right)^{1/2}$ and $\eta > 0$ the control law

$$u_x = \hat{u}_x - \frac{1}{\hat{b}_x} K_x \text{sgn}(S_x) \tag{28}$$

with

$$K_x = \lambda_x\eta + (\lambda_x - 1)|\hat{b}_x\hat{u}_x| \tag{29}$$

ensure the convergence to the sliding surface $S_x = 0$, where S_x and $\hat{u}_x$ are defined in (26) and (27), respectively.

Proof. Similar to Theorem 3.1. □

4. Experimental Characterization

4.1. *Simulations*

In this section the robustness of the proposed sliding mode controller with respect to parameter uncertainty is studied. To this end, the effects of the uncertain value of the curvature k on the total deflection error is analysed using simulations. The block diagram of the control loop used in these simulations is shown in Fig. 3. As shown in this figure, the sliding mode controller and the switching framework are used to find the desired base angle γ^*. The needle base angle is then controlled using a PID controller. The simulations are performed in Matlab/Simulink for different percentage of uncertainty on the nominal value of k. The nominal value of k is selected as 0.0025 mm^{-1} which is added by $\pm 20\%$ uncertainty. Here, the desired path is considered to be a simple 3D curve with zero deflection in the x direction and a curved path in the y direction to avoid an obstacle with a radius of 2 mm at a depth of 80 mm along the y axis. The path can be found using any path planning method. Here the planning method described in [13] is used to find a feasible path. The control signals for x and y nominal averaged subsystem are found using (28) and (19), respectively. Choosing γ^* such that $|\tan\gamma^*| = 1$, the duty cycle periods are calculated from (10) and the PWM framework introduced in 2.2 is used. Fig. 4 shows the norm of the deflection error $\|e\| = \sqrt{e_x^2 + e_y^2}$ at different depths, where e_x and e_y are the difference between the desired path and the needle tip position in x and y directions, respectively. The trend that the error follows highly depends on the desired path and the needle curvature. Here, due to the selection of a desired curved path, nonlinear equations and the nonholonomic constraints, the behavior of the error cannot be predicted. However, as can be seen, for smaller values of curvature, the deflection error is higher. This seems reasonable as it is easier to steer a needle with higher curvature on a curved path. This is only an simple analysis, which cannot be extended to any conclusions. In 4(b), the maximum error for the smallest curvature is larger compared to larger curvatures.

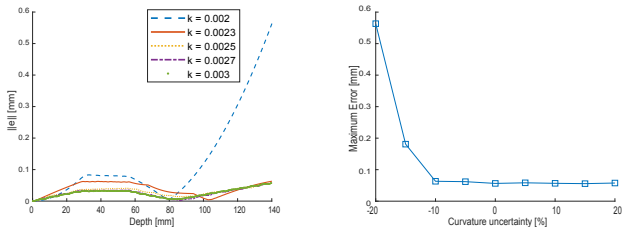

(a) (b)

Figure 4. Simulation results showing the effects of the curvature uncertainty on the system response. (a): The deflection error for different values of k. (b): The maximum deflection error for different values of uncertainty in k.

4.2. *Experiments*

In this section, the performance of the proposed controller implemented in the switching framework introduced in section 2.2 is verified using the experimental setup shown in Fig. 5. The setup is a two stage translational/rotational mechanism. Translational motion is performed by a carriage actuated by a DC motor through a belt and pulley mechanism. Another DC motor is mounted on this carriage which the needle base is attached to and performs needle axial rotation under the direction of a PID controller. The sliding mode controller and the switching framework are implemented using Matlab/Simulink, which interacts with the experimental setup in real-time using xPC Target environment.

Validation is performed by conducting three sets of experiments, each having nine trials. The insertion points for all trials are spaced far enough to prevent any crossing with previous needle tracks in the tissue. The experiments are implemented for two different scenarios. The first scenario is aligned with the main goal of the paper, in which the needle is moved on a straight line and is applicable to brachytherapy procedures. It should be noted that the in this scenario, it is desired to steer the needle on a straight path in 3D space, which is equivalent to keeping the needle deflection in both x and y direction close to zero. Two different plastisol phantom tissues are used in these experiment. These tissues are made of 80% plastic and two different percentage of softener (M-F Manufacturing Co., Fort Worth, TX, USA), 20% and 10% to have tissues with different stiffness. The Young's modulus of elasticity of these tissues are 25 kPa and 40 kPa. The needles used in these experiments are standard 18-gauge brachytherapy needle (Eckert & Ziegler BEBIG Inc., Oxford, CT, USA) made of stainless steel, with an outer diameter of 1.27 mm, an inner diameter of 1 mm, and a bevel angle of approximately 20°. In order to show the ability of the proposed structure for steering the needle on a curved path, in the second scenario, the needle is moved on a pre-planned path, which is applicable in the presence of obstacles on the needle's way to the target. In this scenario, since it is aimed to steer the needle on a curved path, highly flexible notched needles [20] are used. The needle tip position is tracked using 2D ultrasound images (SonixTouch, Ultrasonix, BC, Canada) for visual feedback. In order to use this information in the feedback loop, the visual information is combined with image processing techniques to provide a numerical value using partial observations of the needle. The filter used is a Kalman filter which assumes constant needle change between two successive frames and predicts the needle position in x and y direction. The details about the image processing technique can be found in [21]. The needle tip position is fed back to the controller and is updated every 0.05 sec. The ultrasound probe is attached to a translational platform which tracks the needle tip position.

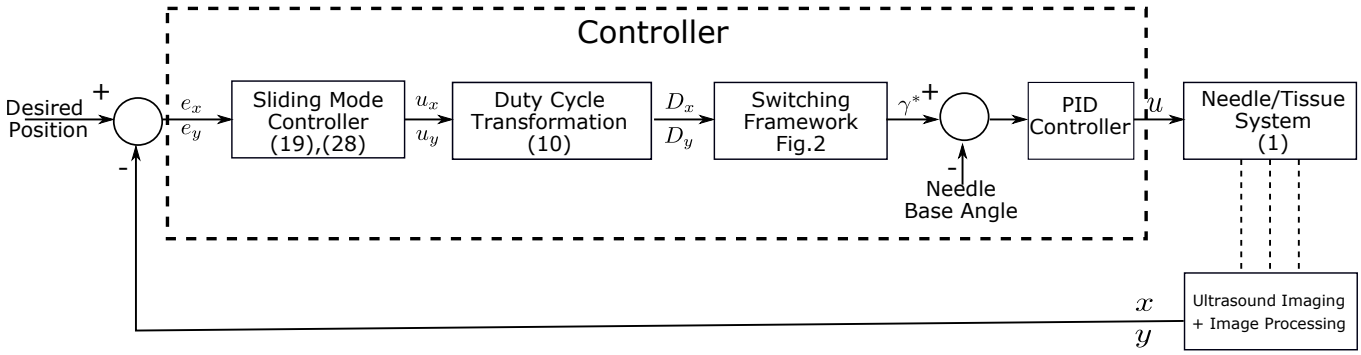

Figure 3. The block diagram of the control loop used in the simulations and experiments.

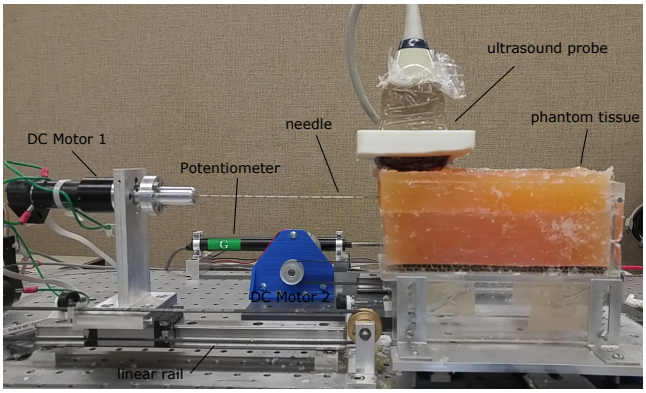

Figure 5. Experimental setup used to perform needle insertion providing translational and rotational motion. The ultrasound machine (SonixTouch, Ultrasonix, BC, Canada) tracks the needle tip position as it is inserted into the tissue. Phantom plastisol tissue is used in these experiments.

Since the needle tip deflection changes are much slower than the noise imposed on the signals, the effect of the noise is reduced by filtering the signals, and the velocity is found by taking the time derivative of the position signal. The trials are performed for a constant insertion velocity of $v = 2$ mm/sec, an insertion depth of 140 mm. Using previous data and pre-operative experiments, the curvature is selected as $0.0024 \leq k \leq 0.0027$ mm^{-1}, which is used in the simulations to find the bounds α^* and β^* as 0.2 rad. γ^* is selected such that $|\tan\gamma^*| = 1$ and the value of the sliding mode parameters ω and η are selected as 0.1 and 0.5, respectively, using simulations and trial and error.

In the first scenario, the desired path is defined as a straight line, which is equivalent to keep the needle deflection in both the x and y directions equal to zero. The results for tissue 1 show a mean absolute error of 0.37 mm in x and 0.3 mm in y. Implementing the same scenario for tissue 2 results in a mean absolute error of 0.28 mm and 0.4 mm for x and y, respectively. Since the control method used here is robust with respect to uncertainties, the errors obtained from two different tissues are in the same order, which shows show that the method does not depend on the tissue parameters.

In the second scenario, it is desired to move the needle on a pre-planned path. The desired path is considered as the same path used in the simulations. The application of this scenario can be observed in obstacle avoidance, where the needle should follow a desired path to go around the obstacle, for example in the case of pubic arch interference (PAI) [22]. The results show a mean absolute error of 0.36 mm and 0.24 mm in the x and y directions, respectively. The maximum targeting error obtained from the experiments is 0.83 mm for x and 1.08 mm for y, as summarized in Table 2. Fig. 6(a), 6(d) and 6(g) represents the results for one of the trials in x-direction from each experimental set. The deflection in y-direction is shown in Fig. 6(b), 6(e) and 6(h), and the four switched modes are shown in Fig. 6(c), 6(f) and 6(i). To have a better idea of the path followed, a 3D plot for one of the trials for case 3 is shown in Fig. 7.

The switching framework proposed in this paper provides the opportunity to use different control strategies. Any controller designed for the two subsystems which satisfies the system constraints, can be used. Here, the sliding mode controller is used as an example to show the effectiveness of the method, however, it is not the only choice. Comparing the results, the maximum error obtained in the experiments is 1.5 mm which is less than 2 mm, the size of the smallest lesion detectable in ultrasound images [23]. The errors are also in the same order of the error in other methods proposed in the literature, like [10], in which the final targeting error is 1.08 mm and 1.3 mm in [14]. This new formulation has the capability to be used with other control strategies to improve the performance, which requires further research.

Table 2. Summary of the experimental results

Case	Tissue	Scenario	x direction				y direction			
			Mean Absolute Error [mm]	Standard deviation σ [mm]	RMSE [mm]	Max Targeting Error [mm]	Mean Absolute Error [mm]	Standard deviation σ [mm]	RMSE [mm]	Max Targeting Error [mm]
1	Tissue 1	Move on a straight line	0.37	0.4	0.48	1.5	0.3	0.31	0.42	0.6
2	Tissue 2	Move on a straight line	0.28	0.26	0.34	0.94	0.4	0.44	0.51	1.4
3	Tissue 1	Obstacle Avoidance	0.36	0.33	0.47	0.83	0.24	0.25	0.34	1.08

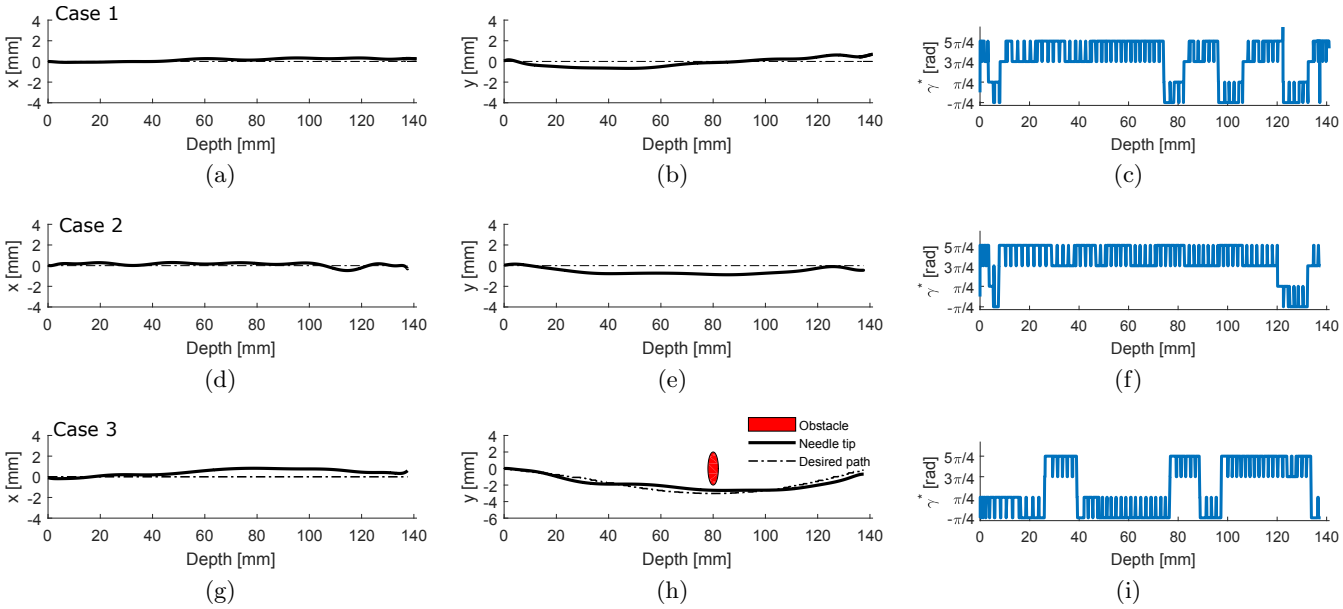

Figure 6. Experimental results presenting the needle tip deflection in one trial for insertion in plastisol tissue with insertion velocity of 2 mm/sec and insertion depth of 140 mm. (a), (b): deflection for tissue 1 and desired path of straight line. (c): angle γ^* determining the switching mode for case 1. (d), (e): deflection for tissue 2 and desired path of straight line. (f): angle γ^* determining the switching mode for case 2. (g), (h): deflection for tissue 1 and desired path of pre-defined curve. (i): angle γ^* determining the switching mode for case 3.

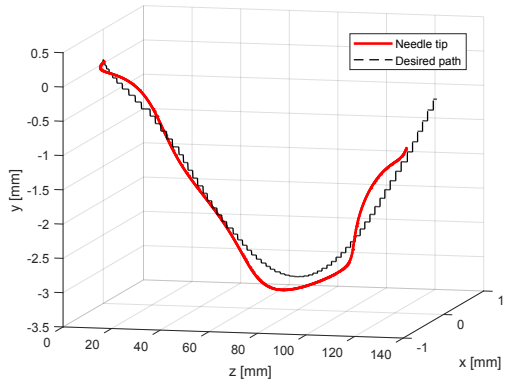

Figure 7. 3D representation of the needle in one of the trials for case 3, following the desired curved path in tissue 1.

5. Concluding Remarks

In this paper, a formulation for transforming the needle steering problem in 3D space into a switching framework is proposed. In this formulation the needle tip deflection is projected into two directions, for which two controllers can be designed independently and translated as duty cycles. The duty cycles are then combined to form a four-mode switching system which simultaneously compensates for deflections in both directions. Later using the sliding mode technique, a robust sliding mode controller is designed for each subsystem and implemented in the proposed switching framework. The proposed method is implemented using an experimental setup for two different scenarios and phantom tissues with different properties. The results show a maximum targeting error of 1.4 mm, which is acceptable in this context and also comparable with other methods proposed in the literature. The proposed framework can be

combined with other available control strategies for minimizing the deflection error. The sliding mode controller proposed here is a conservative method, in which all unknown values are incorporated as uncertainties. However, future works can involve other methods such as model predictive control (MPC) to reduce conservatism and improve performance by optimizing the number of rotations to reduce possible tissue trauma.

Bibliography

[1] K. B. Reed, A. Majewicz, V. Kallem, R. Alterovitz, K. Goldberg, N. J. Cowan, and A. M. Okamura, "Robot-assisted needle steering," *IEEE robotics & automation magazine*, vol. 18, no. 4, pp. 35–46, 2011.

[2] S. Misra, K. B. Reed, B. W. Schafer, K. Ramesh, and A. M. Okamura, "Mechanics of flexible needles robotically steered through soft tissue," *The International journal of robotics research*, 2010.

[3] D. S. Minhas, J. A. Engh, M. M. Fenske, and C. N. Riviere, "Modeling of needle steering via duty-cycled spinning," in *Engineering in Medicine and Biology Society, 2007. EMBS 2007. 29th Annual International Conference of the IEEE*. IEEE, 2007, pp. 2756–2759.

[4] A. Majewicz, J. J. Siegel, A. A. Stanley, and A. M. Okamura, "Design and evaluation of duty-cycling steering algorithms for robotically-driven steerable needles," in *IEEE International Conference on Robotics and Automation (ICRA), 2014*. IEEE, 2014, pp. 5883–5888.

[5] S. Patil, J. Burgner, R. J. Webster, and R. Alterovitz, "Needle steering in 3-d via rapid replanning," *IEEE Transactions on Robotics*, vol. 30, no. 4, pp. 853–864, 2014.

[6] G. J. Vrooijink, M. Abayazid, S. Patil, R. Alterovitz, and S. Misra, "Needle path planning and steering in a three-dimensional non-static environment using two-dimensional ultrasound images," *The International journal of robotics research*, vol. 33, no. 10, pp. 1361–1374, 2014.

[7] P. Moreira, R. Patil, R. Alterovitz, and S. Misra, "Needle steering in biological tissue using ultrasound-base online curvature estimation," in *& International Conference on Robotics and Automation (ICRA), 2014*. IEEE, 2014.

[8] M. C. Bernardes, B. V. Adorno, G. A. Borges, and P. Poignet, "3d robust online motion planning for steerable needles in dynamic workspaces using duty-cycled rotation," *Journal of Control, Automation and Electrical Systems*, vol. 25, no. 2, pp. 216–227, 2014.

[9] J. Chevrie, A. Krupa, and M. Babel, "Needle steering fusing direct base manipulation and tip-based control," in *Robotics and Automation (ICRA), 2016 IEEE International Conference on*. IEEE, 2016, pp. 4450–4455.

[10] A. Krupa, "3d steering of a flexible needle by visual servoing," in *International Conference on Medical Image Computing and Computer-Assisted Intervention*. Springer, 2014, pp. 480–487.

[11] P. Chatelain, A. Krupa, and N. Navab, "3d ultrasound-guided robotic steering of a flexible needle via visual servoing," in *Robotics and Automation (ICRA), 2015 IEEE International Conference on*. IEEE, 2015, pp. 2250–2255.

[12] X. Shen, J. Zhang, E. J. Barth, and M. Goldfarb, "Nonlinear model-based control of pulse width modulated pneumatic servo systems," *Journal of Dynamic Systems, Measurement, and Control*, vol. 128, no. 3, pp. 663–669, 2006.

[13] B. Fallahi, C. Rossa, R. S. Sloboda, N. Usmani, and M. Tavakoli, "Sliding-based switching control for image-guided needle steering in soft tissue," *IEEE Robotics and Automation Letters*, vol. 1, no. 2, pp. 860–867, 2016.

[14] D. C. Rucker, J. Das, H. B. Gilbert, P. J. Swaney, M. I. Miga, N. Sarkar, and R. J. Webster, "Sliding mode control of steerable needles," 2013.

[15] R. J. Webster, J. S. Kim, N. J. Cowan, G. S. Chirikjian, and A. M. Okamura, "Nonholonomic modeling of needle steering," *The International Journal of Robotics Research*, vol. 25, no. 5-6, pp. 509–525, 2006.

[16] V. Kallem and N. J. Cowan, "Image guidance of flexible tip-steerable needles," *Robotics, IEEE Transactions on*, vol. 25, no. 1, pp. 191–196, 2009.

[17] H. D. Taghirad, *Parallel robots: mechanics and control*. CRC press, 2013.

[18] B. Fallahi, C. Rossa, R. Sloboda, N. Usmani, and M. Tavakoli, "Partial estimation of needle tip orientation in generalized coordinates in ultrasound image-guided needle insertion," in *IEEE International Conference on Advanced Intelligent Mechatronics (AIM), 2016*. IEEE, 2016, pp. 1604–1609.

[19] S. J. Dodds *et al.*, "Feedback control," *London: Springer*, p. 5, 2015.

[20] M. Khadem, C. Rossa, N. Usmani, R. S. Sloboda, and M. Tavakoli, "Introducing notched flexible needles with increased deflection curvature in soft tissue," in *Advanced Intelligent Mechatronics (AIM), 2016 IEEE International Conference on*. IEEE, 2016, pp. 1186–1191.

[21] M. Waine, C. Rossa, R. Sloboda, N. Usmani, and M. Tavakoli, "Needle tracking and deflection prediction for robot-assisted needle insertion using 2d ultrasound images," *Journal of Medical Robotics Research*, vol. 1, no. 01, p. 1640001, 2016.

[22] K. Wallner, W. Ellis, K. Russell, W. Cavanagh, and J. Blasko, "Use of trus to predict pubic arch interference of prostate brachytherapy," *International Journal of Radiation Oncology* Biology* Physics*, vol. 43, no. 3, pp. 583–585, 1999.

[23] P. Moreira and S. Misra, "Biomechanics-based curvature estimation for ultrasound-guided flexible needle steering in biological tissues," *Annals of biomedical engineering*, vol. 43, no. 8, pp. 1716–1726, 2015.

Bita Fallahi received her BSc and MSc degrees in electrical engineering from K.N. Toosi University of Technology, Iran, in 2007 and 2011, respectively. She is currently working towards the Doctoral degree in Electrical and Computer Engineering at the University of Alberta and is working on control of robot-assisted minimally invasive surgery. Her current research interests include medical robotics and image-guided surgery.

Ron S. Sloboda received the B.Sc. degree in physics from the University of Manitoba, Winnipeg, MB, Canada, in 1974, and the Ph.D. degree in physics, nuclear theory, from the University of Alberta, Edmonton, AB, Canada, in 1979. He is currently a Professor in the Department of Oncology, University of Alberta. His research interests include dosimetry and treatment planning for brachytherapy, including the design of clinical studies to obtain patient data and model based dose calculation.

Nawaid Usmani's main focus on research is in prostate brachytherapy. Currently, prostate brachytherapy is an increasingly popular treatment option for localized prostate cancer due to its excellent efficacy, good toxicity profile and convenience. However, there remains a great deal of potential to improve the current technique. Dr. Usmani's main objective for this research is to characterize current brachytherapy techniques and identify strategies for improving this treatment. This includes quantifying inaccuracies in current brachytherapy techniques, identifying patient populations at a higher risk of toxicity from this treatment, and finding ways to improve our outcomes with brachytherapy implants (using technical and translational approaches). In addition to this research in prostate brachytherapy, Dr. Usmani is involved in a number of other research endeavours. His other research includes: investigating the potential benefits of metformin in preventing metabolic complications of hormonal therapy and improving prostate cancer outcomes, identifying new prognostic or predictive biomarkers in prostate cancer, investigating the utility of magnetic resonant imaging and PET imaging in the management of prostate cancer, investigating the potential benefits of exercise in rectal cancer patients.

Mahdi Tavakoli is a Professor in the Department of Electrical and Computer Engineering, University of Alberta, Canada. He received his BSc and MSc degrees in Electrical Engineering from Ferdowsi University and K.N. Toosi University, Iran, in 1996 and 1999, respectively. He received his PhD degree in Electrical and Computer Engineering from the University of Western Ontario, Canada, in 2005. In 2006, he was a post-doctoral researcher at Canadian Surgical Technologies and Advanced Robotics (CSTAR), Canada. In 2007-2008, he was an NSERC Post-Doctoral Fellow at Harvard University, USA. Dr. Tavakoli's research interests broadly involve the areas of robotics and systems control. Specifically, his research focuses on haptics and teleoperation control, medical robotics, and image-guided surgery. Dr. Tavakoli is the lead author of Haptics for Teleoperated Surgical Robotic Systems (World Scientific, 2008). He is an Associate Editor for IEEE/ASME Transactions on Mechatronics, Journal of Medical Robotics Research, Control Engineering Practice, and Mechatronics.